Research Square

Preprints are preliminary reports that have not undergone peer review.
They should not be considered conclusive, used to inform clinical practice,
or referenced by the media as validated information.

A Pre-Loaded, Pre-Moistened Foundation for Sabkha Soil: Schedule-Overlap Innovation Using Coupled Boundary-Value/Transient Infiltration Analysis

Naif Alsanabani

nalsanabani@ksu.edu.sa

Nesma and Partners' Chair for Construction Research and Building Technologies, Department of Civil Engineering, College of Engineering, King Saud University

Khalid AL-Gahtani

Nesma and Partners' Chair for Construction Research and Building Technologies, Department of Civil Engineering, College of Engineering, King Saud University

Abdulrahman Bin Mahmoud

Nesma and Partners' Chair for Construction Research and Building Technologies, Department of Civil Engineering, College of Engineering, King Saud University

Salman Akhtar

Nesma and Partners' Chair for Construction Research and Building Technologies, Department of Civil Engineering, College of Engineering, King Saud University

Article

Keywords: sabkha, collapsible soil, wetting-induced collapse, pre-loaded foundation, Green-Ampt infiltration, schedule-overlap

Posted Date: August 3rd, 2026

DOI: https://doi.org/10.21203/rs.3.rs-9927844/v1

License: This work is licensed under a Creative Commons Attribution 4.0 International License.
Read Full License

Additional Declarations: No competing interests reported.

Version of Record: A version of this preprint was published at Scientific Reports on October 13th, 2026. See the published version at https://doi.org/10.1038/s41598-026-75434-y.

A Pre-Loaded, Pre-Moistened Foundation for Sabkha Soil: Schedule-Overlap Innovation Using Coupled Boundary-Value/Transient Infiltration Analysis

Naif Alsanabani, Khalid Al-Gahtani, Abdulrahman Bin Mahmoud, Salman Akhtar

Corresponding Author: Naif Alsanabani (nalsanabani@ksu.edu.sa)

Abstract

Conventional improvement methods applied to sabkha soil (collapse soil) are time-consuming, lengthening the project schedule. This paper introduces a pre-loaded, pre-moistened shallow foundation that deliberately triggers the collapse mechanism under controlled construction conditions. A single-footing cast directly on dry sabkha incorporates a 3×3 array of vertical holes through which distilled water is introduced, advancing as a Green-Ampt wetting front and dissolving the evaporitic bonds before superstructure load application. The improvement phase overlaps temporally with foundation construction, thereby removing the improvement task from the critical path, as per the schedule overlap principle. A coupled boundary-value problem (Terzaghi consolidation) and a transient infiltration problem are developed to model consolidation and collapse settlement due to wetting, and they are verified against a plane-strain elastic stress analysis and a one-dimensional coupled hydro-mechanical Richards-BBM model. Results show that the innovative foundation mobilizes approximately 501 mm of collapse settlement within 12 days under early-construction loading (before the superstructure is placed), which corresponds to the full wetting-induced collapse under self-weight, leaving negligible post-commissioning settlement. In contrast, a conventional foundation subjected to accidental inundation exhibits a settlement of 728 mm. The schedule overlap reduces the pre-superstructure phase by 62% compared with traditional pre-wetting..

Keywords: sabkha; collapsible soil; wetting-induced collapse; pre-loaded foundation; Green-Ampt infiltration; schedule-overlap

1. Introduction

Sabkha are evaporite-cemented soils that blanket vast swathes of the Arabian Gulf coastline, from the Sebkhet Bou Areg in Morocco through the Khor Al-Zubair in Iraq and, most extensively, along the shores of Saudi Arabia, the United Arab Emirates, Qatar, Bahrain, and Kuwait. Their engineering behavior is governed by a chemically precipitated network of halite, gypsum, and anhydrite crystals that binds an otherwise loose quartz skeleton into a rigid, desiccated matrix. The resulting unsaturated fabric displays a deceptively high dry strength that is highly sensitive to the salinity, temperature, and relative humidity of the pore fluid. Whenever the matric suction is reduced, the soluble bridges dissolve, and the skeleton collapses under even modest stresses,

delivering the wetting-induced volumetric strain that has made sabkha notorious in the foundation engineering literature [1], [2], [3]

Recent reviews and case studies show that a wide range of ground-improvement techniques (replacement, compaction, chemical stabilizers, nanomaterials, industrial by-products, and biopolymers) can markedly reduce the potential for collapse and increase the bearing capacity of collapsible soils, but rarely eliminate the risk of collapse. [4], [5]. Even after treatment, collapsible and gypseous soils remain highly sensitive to changes in moisture and suction, so significant additional settlements can occur if the groundwater table rises, drainage is modified, or water accumulation persists near foundations during service life. [6], [7]. Field and laboratory evidence from loess and gypseous soils illustrates that wetting episodes or prolonged ponding after construction can still trigger substantial volume reduction and serviceability problems, underscoring the need to design improvement schemes and surface/groundwater management together rather than treating ground improvement as a complete removal of collapse hazard ([6]

The present paper reframes the problem. Rather than eliminate the collapse mechanism, the proposed foundation deliberately triggers it under its own dead weight during a controlled wetting phase that overlaps with the foundation's structural works. According to Figure 1, a shallow strip footing is cast directly on the dry sabkha with a 3x3 array of small-diameter vertical holes that pass through the foundation thickness into the soil below. Once the foundation has gained nominal structural strength, distilled water is introduced through the holes, advancing as a Green-Ampt wetting front into the sabkha layer, dissolving the evaporitic bonds, and producing the majority of the soil improvement before the superstructure load is applied. Because the improvement time is absorbed into the foundation construction time, it is effectively removed from the critical path. The principle is denoted here as the schedule-overlap principle, by analogy with the overlap concept routinely used in construction management. [8].

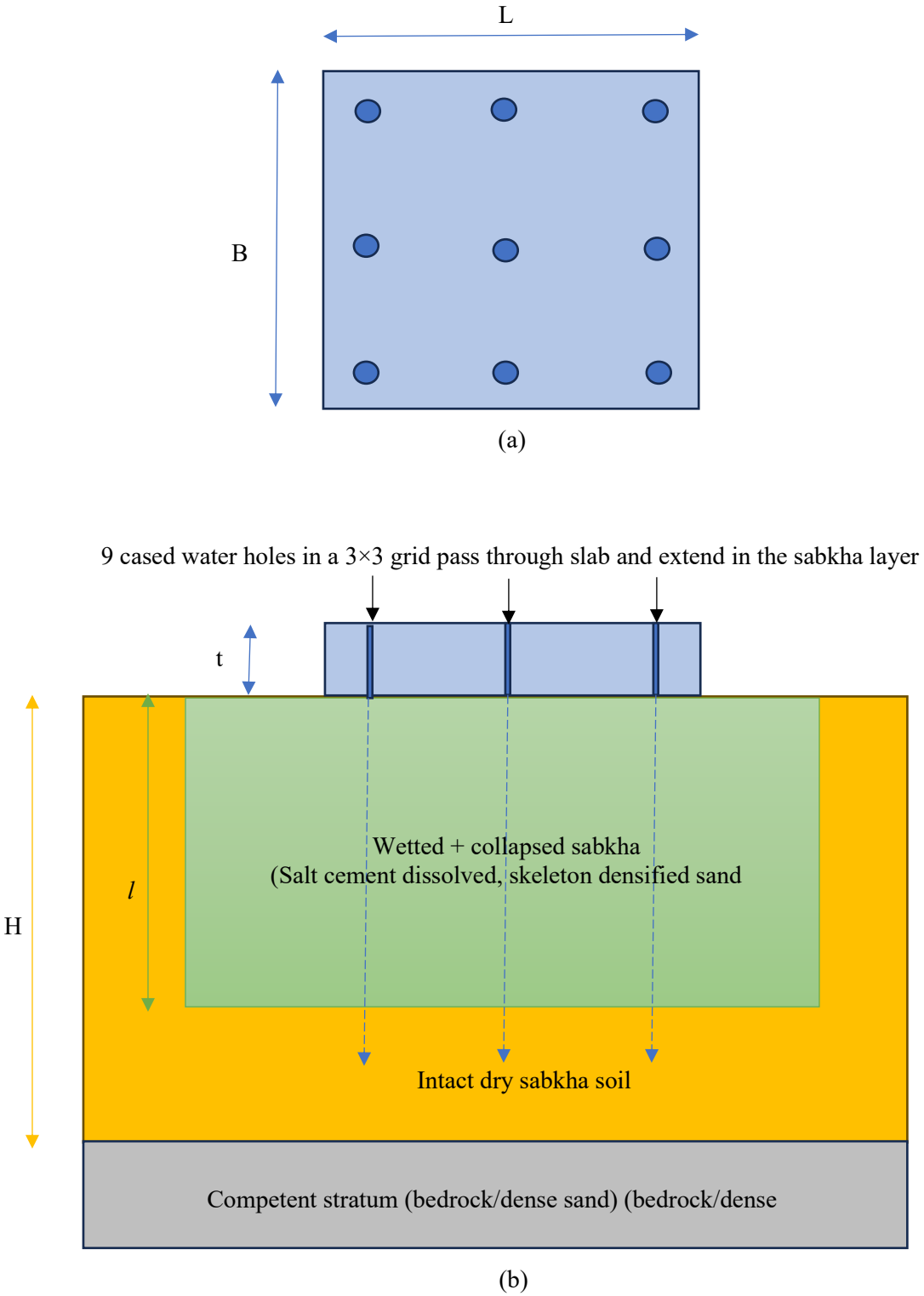


Figure 1: configuration of the innovative foundation (a) plan view of the foundation, (b) schematic cross-section

Four research questions structure the paper: (i) how much post-commissioning settlement does the innovative method inherit relative to a conventional, dry-state foundation exposed to an accidental wetting event; (ii) how does the time-evolving bearing capacity compare with that of an untreated, flooded footing; and (iii) how much project time is saved by overlapping the improvement phase with the foundation works? The paper addresses these questions through a coupled boundary-value/transient-value analytical framework, verified against a plane-strain elastic stress analysis. The analytical scope is intentionally analytical-numerical; a dedicated physical model and full-scale field verification program are the subject of a companion study. The paper's main contributions are (i) delivering the controlled pre-wetting pulse through the foundation hardware itself—unlike conventional pre-inundation or permeation methods, this approach absorbs the soil-improvement phase entirely into the foundation-construction window, removing it from the critical path while exhausting the deposit's wetting-induced collapse potential before any superstructure load is applied; and (ii) a coupled boundary-value/transient infiltration analytical framework that quantifies the resulting schedule-overlap benefit and post-commissioning settlement for collapsible sabkha soils.

2. Literature review

2.1 Genesis, mineralogy, and engineering behavior of sabkha

Sabkha soils are the product of repeated evaporative cycles on coastal flats where groundwater capillarity draws saline fluid to the surface, and mineral salts precipitate interstitially. The soluble minerals, halite and gypsum in particular, are highly reactive and thermodynamically unstable in fresh water. The classical engineering characterization was established by Akili and Ahmed [9] and Al-Amoudi [10], who documented the dry-state strength enhancement produced by the evaporite cementation and the dramatic loss of strength upon flushing with non-saline water. Al-Otaibi and Aldaihani [2] reported collapse potentials in the range 6-22 percent, and demonstrated that the compression index can more than double as the soil passes from the cemented to the decemented state.

Collapsible soils in arid and semi-arid regions often show high apparent strength and stiffness in the natural, unsaturated state because of open metastable structures bonded by suction and/or soluble salts. Still, they can undergo sudden, large volume reduction when wetted under load [11], [12], [13]. In saline sabkha and other salt-affected collapsible soils, wetting or sustained

percolation of water dissolves cementing salts and reduces suction, leading to breakdown of the skeleton and significant settlement, even though conventional oedometer flooding may underestimate this collapse potential [14]. Laboratory and field studies on sabkha, loess, and gypseous or salty collapsible soils consistently show that changes in groundwater level, drainage, or hydrological boundary conditions (e.g., drying–wetting cycles, salt washing/supplying, infiltration from surface water or infrastructure) can progressively degrade stiffness and increase collapse or settlement, so that substantial deformation may still occur long after initial construction or treatment if the moisture regime changes [15], [16], [17]. As a result, ground-improvement and stabilization measures (such as compaction, salt- or gypsum-based stabilization, or other chemical/physical treatments) can reduce but do not eliminate the risk of wetting-induced collapse, and long-term performance remains highly dependent on controlling water table and drainage conditions [13], [2]

2.2 Conventional ground improvement for collapsible soils

Several techniques have been proposed to mitigate the potential for collapse in collapsible soils, with pre-construction soil improvement proving particularly effective. Increasing relative compaction and saturation levels before construction can significantly reduce the potential for collapse and associated risk. [18]. Additionally, pre-wetting combined with compaction, as well as partial replacement with compacted sand or crushed stone layers beneath shallow footings, helps reduce collapse and improve bearing capacity upon inundation. [19].

Beyond these approaches, dynamic compaction has been shown to greatly enhance compressibility and reduce collapse potential in gypseous (collapsible) soils, with the degree of improvement increasing with gypsum content and appropriate blow counts and drop heights [4]. Regarding column-based interventions, simple sand columns offer little control over wetting-induced collapse. In contrast, geosynthetic-encased stone or sand columns markedly reduce or even prevent collapse under inundation while allowing higher applied stresses. [4], [20], [21], [22].

2.3 Analytical and numerical modeling of wetting-induced collapse

Analytical prediction of wetting-induced collapse often proceeds in an uncoupled way: infiltration is described by a Green–Ampt–type wetting front, possibly modified for complex boundary conditions, while settlement is obtained from 1D consolidation/void-ratio–suction relationships or collapse indices derived from oedometer and soil-water characteristic curves. [23], [24], [25],

[26]. Terzaghi-style 1D formulations remain the backbone for vertical strain computation, with collapse incorporated via suction-dependent volumetric strain or void-ratio changes calibrated from laboratory tests. [23], [24].

Fully coupled hydro-mechanical models based on the Barcelona Basic Model and its extensions (e.g., BBM, BExM, EBBM, hypoplastic variants) capture suction-dependent stiffness, strength, and wetting collapse more rigorously, and have been used to simulate rainfall- or groundwater-induced settlements of shallow foundations and loess deposits. [27], [28], [29], [30], [31]. Benchmarking exercises show that BBM-type models require substantial parameter calibration from specialized tests. [32].

Recent studies employ 2D/3D finite-element or finite-volume hydro-mechanical (HM) models that couple Richards-type flow with BBM/EBBM-type constitutive laws to reproduce measured collapse settlements of shallow foundations and infiltration test results. [27], [28], [30]. These works highlight the need for consistent calibration against double-oedometer tests, SWCCs, and field data, but also demonstrate good agreement between simulated and observed long-term settlements and collapse potentials. [27], [28], [30].

2.4 Gap knowledge

A common limitation of published frameworks is that they treat the soil-improvement task as an independent, serial activity and therefore cannot capture constructability innovations that overlap soil improvement with foundation construction. Shillaber et al. [33] explicitly acknowledged this gap when noting that schedule-driven constraints can override sustainability rankings and recommended that future frameworks incorporate construction-sequence flexibility as a first-class variable. Raymond et al. [34] shared this recommendation by calling for the inclusion of schedule-related indirect costs in life-cycle sustainability assessments of ground-improvement methods. The present study addresses both recommendations by combining (i) a deterministic, mechanics-based prediction of post-commissioning settlement, and (ii) a schedule-overlap module that decomposes the critical path into parallel rather than serial tasks.

3. Methodology

The analytical framework comprises six interconnected modules executed sequentially and coupled through the wetting-front position and the foundation stress field. The modules are: (i)

parameter collection from the laboratory and literature; (ii) Terzaghi one-dimensional consolidation boundary-value problem (BVP) solved by eigenfunction expansion; (iii) Green-Ampt transient infiltration model tracking the wetting front below the nine-hole array; (iv) Meyerhof bearing-capacity calculation for dry, wetted, and post-improvement states; (v) Duncan-Chang hyperbolic load-settlement curve; and (vi) Boussinesq plane-strain elastic stress verification. A seventh module performs schedule performance analysis. Each module is described below.

3.1 Soil model parameters

The soil profile is idealized as a single sabkha layer of thickness H = 4.0 m, underlain by an impermeable base, and overlaid by a 0.5 m embedment of the innovative footing with width B = 2.0 m. All parameters are representative of the Arabian Peninsula sabkha as reported in Al-Amoudi [35]. Table 1 summarises the parameter set for the dry (in-situ), wetted, and post-improvement states. The post-improvement state represents the pre-loaded, densified skeleton that remains once the wetting-induced collapse under the foundation's early-construction loading has been exhausted; its compression index is taken as 0.08 based on the post-collapse oedometer curves reported .

Table 1. Geotechnical parameters for sabkha *[12], [36].*

Parameter	Symbol	Dry	Wetted	Post-imp.	Unit
Young's modulus	E	12,000	2,500	5,000	kPa
Coefficient of consolidation	c_v	2.0e-6	4.5e-6	4.5e-6	m2/s
Compression index	Cc	0.18	0.42	0.10	-
Initial void ratio	e_0	0.85	-	-	-
Friction angle	$\emptyset$	35	24	33	deg
Cohesion	c	25	5	9	kPa
Collapse potential	CP	12	-	-	%
Vertical hydraulic conductivity	k_v	-	5e-8	-	m/s
Unit weight	γ	16.5	-	-	kN/m3
Layer thickness	H	4.0	-	-	m
Footing width	B	2.0	-	-	m
Applied stress	q	100	-	-	kPa

3.2 Terzaghi consolidation boundary-value problem

Consolidation settlement is governed by Terzaghi's one-dimensional diffusion equation for the excess pore pressure u(z, t), Eq. (1)

$$\frac{\partial u}{\partial t} = C_v \frac{\partial^2 u}{\partial z^2} \quad (1)$$

with boundary conditions u(0, t) = 0 (drained top) and du/dz at z = H equal to zero (impermeable base), and initial condition u(z, 0) = q_0 = 100 kPa. This stress represents the total construction-phase load comprising the weight of the reinforced concrete footing, formwork, reinforcement cage, and early gravity loads transferred to the foundation during the concurrent wetting phase; it is the load present while the soil undergoes wetting-induced collapse, not the full superstructure service load that is applied afterward. The wetting-induced collapse settlement (Section 3.3) is driven independently by suction change from wetting and is not a direct function of the applied stress. Accordingly, the initial condition u(z, 0) = q_0 corresponds to a construction-phase applied stress q_0 = 100 kPa. The analytical solution is obtained by separation of variables and Fourier sine expansion, Eq. (2)-(4).

$$u(z,t) = \sum_n \frac{2q_0}{M} sin\left(\frac{Mz}{H}\right) exp(-M^2 T_v) \quad (2)$$

$$M = \frac{(2n+1)\pi}{2} \quad (3)$$

$$T_v = \frac{c_v t}{H^2} \quad (4)$$

The degree of consolidation U(Tv) is obtained by integration over the layer depth, Eq. (5)

$$U(T_V) = 1 - \frac{8}{\pi^2} \sum_n \frac{exp(-M^2 T_v)}{M^2} \quad (5)$$

The series is truncated at N = 60 terms, which yields convergence better than 0.01 percent over the full range of Tv. The ultimate consolidation settlement (S_{ult}) is obtained from the compression index, Eq. (6).

$$S_{ult} = \frac{C_c H}{1+e_0} log\left(\frac{\sigma_0' + q_0}{\sigma_0'}\right) \quad (6)$$

Eq. (6) is evaluated in three states: dry with Cc = 0.18, wetted with Cc = 0.42, and post-improvement with Cc = 0.10. The coefficient of consolidation (cv_{wet}) for the wetted state is larger than for the dry state (cv_{dry}) (cv_{wet}= 4.5e-6 m^2/s versus cv_{dry}= 2.0e-6 m^2/s), because the wetting destroys the salt cementation and increases the permeability faster than it increases the compressibility.

3.3 Wetting-front propagation and wetting-collapse constitutive model

3.3.1 Green-Ampt wetting-front transient infiltration problem

Infiltration through the nine vertical holes is modeled as a one-dimensional advancing wetting front with ponded water at the inlet. The infiltration rate $f(t)$ and cumulative infiltration $F(t)$ are related by Eq. (7)-(9).

$$f(t) = k_v \frac{H_P + \psi_f + L_f}{L_f} \tag{7}$$

$$\frac{dL_f}{dt} = \frac{f(t)}{\Delta_\theta} \tag{8}$$

$$\Delta_\theta = \theta_s - \theta_r \tag{9}$$

where L_f is the wetting-front depth (m); k_v = 5e-8 m/s is the effective vertical hydraulic conductivity of the nine-hole array; ψ_f= 0.30 m is the matric suction head at the wetting front; H_P = 0.05 m is the ponded head above the inlet; and θ_s = 0.45 and θ_r= 0.05 are the saturated and residual volumetric water contents. The ODE in Eq. (8) is integrated by an iterative Picard scheme with sub-day time steps ($\Delta t \leq 0.1$ day), consistent with the Richards solver described in Section 3.3.2. The fraction of the sabkha layer wetted at any time is defined as $\alpha(t)$, Eq. (10).

$$\alpha(t) = Min\left(\frac{L_f(t)}{H}, 1\right) \tag{10}$$

The effective vertical hydraulic conductivity of the nine-hole array is taken as $k_e = k_v \times 2.62$, which accounts for the combined contribution of the nine holes and the lateral redistribution of infiltrated water between them; the 3×3 arrangement was selected to provide uniform lateral coverage of the footing plan area.

3.3.2 SWCC-driven wetting-collapse constitutive model and coupled hm validation

Following the Section 2.3 review, the analytical wetting-collapse settlement is computed in an uncoupled way that closes the gap between the Green-Ampt suction history and a constitutive collapse strain calibrated against the double-oedometer test. The soil-water characteristic curve (SWCC) is described with the modified Fredlund-Xing with residual water content, Eq. (11), in which the volumetric water content $\theta(\psi)$ is a function of the matric suction ψ through the scale a, the slope n, the curvature m and the residual-suction parameter ψ_r. The effective saturation $Se(\psi) = (\theta - \theta_r)/(\theta_s - \theta_r)$ follows directly from Eq. 11, 12 [37].

$$\theta(\psi) = \left[\theta_r + \frac{(\theta_s - \theta_r)}{\left[ln\left(e + \left(\frac{\psi}{a}\right)^n\right)\right]^m}\right] \times C(\psi) \quad (11)$$

$$C(\psi) = \frac{1 - ln\left(1 + \frac{\psi}{\psi_r}\right)}{ln\left(1 + \frac{10^6}{\psi_r}\right)} \quad (12)$$

The wetting-collapse strain at every horizontal slice is taken as a linear function of the change in effective saturation between the in-situ state ψ_0 and the current state ψ(z, t), Eqs. 13, 14. The proportionality constant is the laboratory-measured collapse potential CP from the double-oedometer test, so the model preserves the asymptotic value CP·H at full saturation. Pereira and Fredlund [38] use a curvature-of-SWCC formulation.

$$S_e(\psi) = \frac{(\theta - \theta_r)}{(\theta_s - \theta_r)} \quad (13)$$

$$\varepsilon_c(\psi) = \frac{CP \times [S_e(\psi) - S_e(\psi_0)]}{[1 - S_e(\psi_0)]} \quad (14)$$

The wetting-collapse settlement of the layer is then the depth integral of ε_c over the column, Eq. 15 where the suction profile $\psi(z, t)$ is derived from the Green-Ampt smoothed by a tanh transition of half-width δ = 0.05 m. This uncoupled SWCC + double-oedometer formulation requires no extra calibration tests beyond those already used by Eq. (6) and is consistent with the SWCC-based wetting-collapse predictions [38], [39].

$$S_{collapse}^{ana}(t) = \int_0^H \varepsilon_c\big(\psi(z, t)\big)\, dz \quad (15)$$

To verify the analytical pipeline, an independent one-dimensional coupled hydro-mechanical (HM) numerical model is implemented in the same Python notebook. The unsaturated flow is governed by the Richards equation in mixed [40] form, Eq. 16, with $C(\psi) = -d\theta/d\psi$ obtained from the same Fredlund-Xing SWCC and the relative permeability (Mualem-style closure) [40].

$$C(\psi)\frac{\partial \psi}{\partial t} = \frac{\partial}{\partial z}\left[K(\psi)\left(\frac{\partial \psi}{\partial Z} - 1\right)\right] \quad (16)$$

The mechanical update follows the Barcelona Basic Model [41] loading-collapse (LC) idea: every suction decrease past the previous minimum activates a plastic volumetric strain increment, Eq. 17, where p_{atm}= 100 kPa is the atmospheric reference, and ψ_{min}^{old}, ψ_{min}^{new} are the running suction minima before and after the time step [41].

$$\Delta\varepsilon_v^p(z,t) = \frac{CP}{ln\left(\frac{\psi_0+p_{atm}}{\psi_{top}+p_{atm}}\right)} ln\left(\frac{\psi_{min}^{old}+p_{atm}}{\psi_{min}^{new}+p_{atm}}\right) \quad (17)$$

where $\Delta\varepsilon_v^p(z,t)$is an incremental plastic (irreversible) volumetric collapse strain at depth $z$and time t, $e_0$is an initial void ratio. $\psi_{\min}, \psi_{\min}$is a minimum historical suction before and after the current wetting increment.

The solver uses 41 nodes (Δz = 0.10 m), a semi-implicit Picard time integration with Δt = 600 s, a Dirichlet ponding condition ψ = ψ_{top} = 0.5 kPa at the surface and a no-flow Neumann condition at the impermeable base. The wetting-collapse settlement is the depth-integral of the accumulated $\Delta\varepsilon_v^p(z,t)$. The Richards + BBM-LC settlement-time history is benchmarked against the analytical SWCC + oedometer prediction over the first 180 days. The two models reach the CP·H asymptote with a normalized RMSE of approximately 5.6 percent (final analytical 477 mm, final numerical 456 mm against the CP·H reference of 480 mm), and the numerical model captures a slightly more diffused front than the sharp-interface Green-Ampt analytical prediction, as shown in Figure 2. The agreement is consistent with the BBM-type benchmarking results reviewed in Section 2.3 and confirms that the uncoupled analytical pipeline is fit-for-purpose for the foundation design study reported in Sections 4 and 5.

Validation

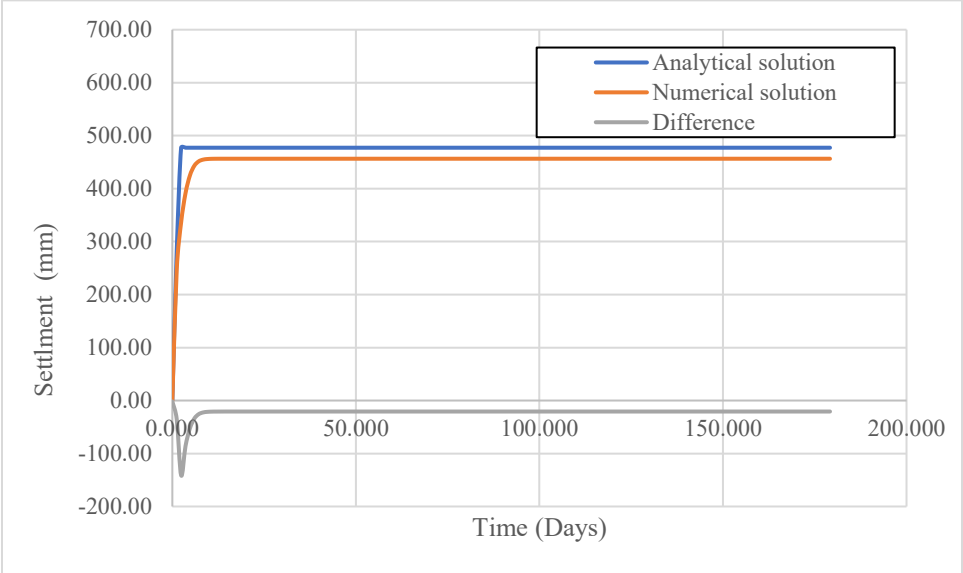


Figure 2. Analytical and numerical results of the collapse settlement

3.4 Duncan-Chang hyperbolic load-settlement model

After the soil collapse process is completed under wetting and foundation loading, and the foundation has reached a steady state, the foundation's nonlinear load-settlement response is characterized by the hyperbolic model of Duncan and Chang [42], Eqs. (18)- (20).

$$S(q) = \frac{q}{a+bq} \tag{18}$$

$$a = \frac{1}{k_i} \tag{19}$$

$$b = \frac{R_f}{q_u} \tag{20}$$

where k_i is the initial subgrade modulus (kPa/mm), R_f is the failure ratio and set as 0.85, and $q_u$is the Meyerhof ultimate capacity, which is computed in Eq (21).

$$q_u = c \times N_c \times s_c \times d_c + q \times N_q \times s_q \times d_q + 0.5 \times \gamma \times B \times N_\gamma \times s_\gamma \times d_\gamma \tag{21}$$

where N_c, N_q, and N_γ are bearing number factors, s_c, s_q, and s_γ are shape factors, d_c, d_q, and d_γ are depth factors. The model is evaluated in the dry, wetted, and post-improvement states using the corresponding E and q_u.

3.5 Boussinesq plane-strain elastic stress verification

The analytical pipeline is verified by a plane-strain elastic stress analysis in which the vertical stress increment beneath a uniformly loaded strip footing is computed from the closed-form Boussinesq [43], [44] solution, Eq. (22).

$$\Delta\sigma_z = \frac{q(\alpha+sin(\alpha)\cos(\alpha+2\beta))}{\pi} \tag{22}$$

with α and β the half-angles subtended by the footing edges at the stress point (x, z). A structured 20 x 16 grid of Q4 isoparametric points is evaluated at the element centroids over a 6.0 m by 10.0 m domain, and the depth-integrated vertical strain is compared with the analytical consolidation settlement. A staged procedure is used: stage 0 applies the full 100 kPa on the dry soil; stages 1-18 advance the wetting front in increments of H / 18 and reassign the affected elements from dry to wet moduli, reassembling the equivalent stiffness at every stage. Wetting-induced collapse is introduced as a prescribed vertical compressive eigenstrain equal to CP / 100 on each newly wetted element; the equivalent nodal force vector is obtained by the virtual-work principle, Eq. (23).

342 $$F^{eq}(e) = \int_{-1}^{1}\int_{-1}^{1} B^T D\varepsilon_c |J| d\xi d\eta \quad (23)$$

343

344 where B is the strain-displacement matrix, D the plane-strain constitutive matrix, and $|J|$ the
345 Jacobian determinant. Bottom nodes are fixed and lateral nodes are restrained horizontally (roller).
346 The discrete system is solved by direct Gaussian elimination at each stage. Table 2 summarizes
347 the finite-element parameters.

348 **Table 2.** Plane-strain elastic stress analysis parameters.

Parameter	Value
Element type	Q4 isoparametric plane-strain
Mesh dimensions	20 x 16 = 320 elements, 357 nodes
Domain size (width x depth)	6.0 m x 10.0 m
Number of wetting stages	18
Wetting increment per stage	H / 18 = 0.556 m
Penalty stiffness	1×10^{14} kN/m
Gauss integration order	2 × 2 per element
Collapse formulation	initial-strain (eigenstrain) method
Stiffness reassembly	full reassembly at every stage
Equation solver	direct Gaussian elimination

349 **3.6 Schedule-overlap principle and critical-path duration**

350 The construction duration is decomposed into three tasks: soil improvement ($T_{improve}$), foundation
351 construction (T_{found}), and superstructure erection (T_{super}). For a serial schedule (conventional),
352 the critical-path duration is simply the sum, while for a parallel schedule (innovative),
353 improvement and foundation construction are carried out concurrently, Eq. 24 and 25,
354 respectively.

355 $$T_{cp-serial} = T_{improve} + T_{found} + T_{super} \quad (24)$$

356 $$T_{cp-parallel} = max\left(T_{improve}, T_{found}\right) + T_{super} \quad (25)$$

357 The time saving (ΔT) can be computed as $\Delta T = T_{cp-serial} - T_{cp-parrallel}$ translates directly to
358 savings on site overhead and lost revenue.

359 **4. Results and discussion**

360 The results of the innovative foundation are displayed in two aspects as geotechnical behavior and
361 construction performance.

4.1 Geotechnical behavior of the innovative foundation

4.1.1 Settlement-time behavior

Figure 3 plots the 5-year cumulative settlement of three foundation states: (i) the innovative pre-loaded and pre-wetted foundation; (ii) the conventional foundation resting on dry sabkha that is never subjected to a wetting event; and (iii) the conventional foundation on dry sabkha that experiences a sudden in-service inundation (e.g. a service-water leak or a seasonal rise of the saline groundwater table). The innovative curve rises from an instantaneous elastic settlement of about 76 mm at t = 0 to approximately 577 mm by day 12, corresponding to almost the full wetting-collapse increment of 480 mm computed from the closed-form CP·H reference, and then asymptotes at 594 mm by day 60, after which it remains essentially flat for the remaining 4 years and 9 months of the simulation.

The final settlement of the conventional dry foundation experiences is 248 mm, including the immediate and consolidation settlement, with a compression index Cc of 0.182 mm. The conventional foundation that is suddenly inundated, by contrast, follows the dry-state curve until the flood event, after which it suffers an additional step increase of approximately 480 mm and a long consolidation tail under the wet-state compression index C_c = 0.42, terminating at 728 mm, almost three times the dry-no-flood settlement and 134 mm above the innovative case. The engineering message is that the 594 mm of strain delivered to the innovative foundation is consumed during construction stage, before the superstructure is placed, whereas the 480 mm collapse step under the inundated conventional foundation is delivered to the structure in service, with all the attendant distortion, cracking and loss-of-use consequences for the supported building.

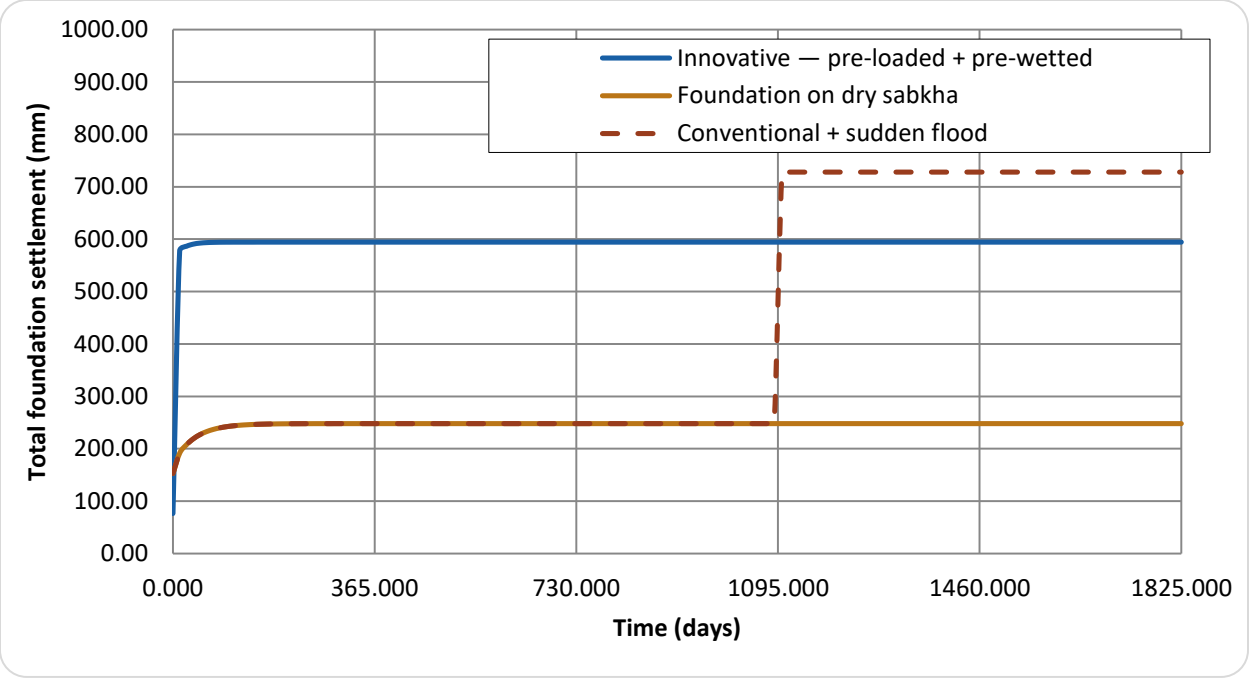


Figure 3. Time history settlement of the innovative foundation and foundation in dry and wet conditions

The three-regime shape of the innovative curve, an initial elastic step, a rapid wetting-collapse phase, and a flat long-term plateau, is consistent with the staged-wetting laboratory and field measurements reported by Al-Amoudi and Abduljauwad [12] and Akili and Ahmad [9] for Arabian Gulf sabkha, and by Pereira and Fredlund [38] for compacted gneiss residual soils, they showed that the bulk of the wetting-induced collapse is mobilized once the wetting front has traversed the cemented horizon and that subsequent wetting events under post-collapse stress produce only marginal additional strain. The 480 mm step suffered by the conventional foundation when accidentally flooded is consistent with the wetting-induced collapse mechanism documented by Hou, Vanapalli and Li [24] for the irrigation-induced wetting-front propagation in collapsible loess deposits at Heifangtai, where the bulk of the wetting-induced subsidence develops once the wetting front fully traverses the cemented horizon. Opukumo et al. [11] emphasized that the dominant risk for arid-region foundations is precisely this in-service flooding scenario, and that the only robust mitigation is the controlled pre-wetting of the deposit before the structural load is applied, the principle realized in the present innovative scheme. The 134 mm advantage of the innovative method over the conventional-with-flood case is due to gradual breaking of particle bonding.

4.1.2 Wetting-front depth and wetted fraction

Figure 4 traces the Green-Ampt wetting-front depth $L_f(t)$ and the corresponding wetted fraction $\alpha(t) = L_f/H$ of the 4 m sabkha layer beneath the innovative foundation. The wetting front advances rapidly during the early injection phase, reaching the upper 1 m within the first 24 hours, propagating through 2 m by approximately day 4, and traversing the full 4 m layer thickness by day 12. After day 12, the front depth L_f is locked at the layer base ($L_f = H = 4$ m) and the wetted fraction α saturates at unity for the remainder of the simulation. The shape of the *L_f-time* curve is the analytical signature of one-dimensional vertical infiltration into a sandy-silt matrix under a sustained ponded boundary at the surface and a no-flow base condition: an early square-root-of-time advance dominated by the matric-suction gradient at the front, followed by a near-linear gravity-dominated advance once the saturated column above the front has exceeded the suction head ψ_f. The wetted-fraction curve, being the volumetric counterpart of $L_f(t)/H$ for a uniform layer, follows the same trajectory and reaches unity at $t = 12$ days. The 12-day full-saturation interval is approximately one order of magnitude shorter than the 90–120 day duration assumed in the Traditional Pre-Wetting baseline, which is the kinematic origin of the schedule-overlap saving quantified in the later section. Second, because α reaches unity at early times, the wetting-induced collapse occurs entirely under the early-construction loading (before the superstructure is placed), rather than under the service load—which explains the essentially flat post-commissioning settlement plateau in Figure 3.

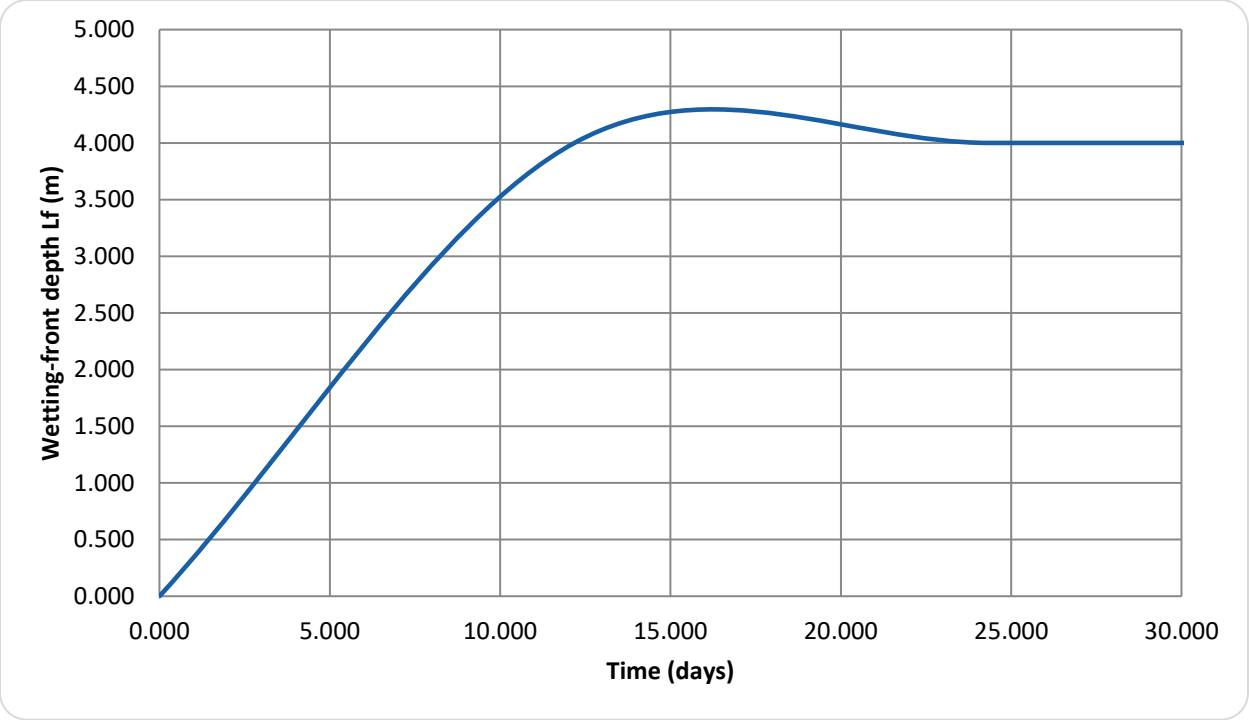


Figure 4. Green-Ampt wetting-front depth and wetted fraction

The above result is consistent with the analytical framework reviewed by Adem and Vanapalli [45] for the prediction of in-situ volume change in unsaturated soils, and with the improvements to the Green-Ampt model proposed by Chen et al. [26] for slope-scale infiltration analyses of progressive water damage. The 12-day full-saturation interval reported here is markedly longer than the multi-hour wetting-front advance times reported by Yao et al. [29] for stratified rainfall-infiltration cases on natural slopes (e.g., approximately 100 hours for the wetting front to traverse a 5.8 m slip surface under a rainfall intensity of 30 mm/h), a difference attributable to the much higher imposed-head boundary used in the present injection scheme (≈ 4 m of ponded distilled water versus rainfall fluxes on the order of 30 mm/h), and is consistent with the field-scale wetting-front advance documented by Hou et al. [24] for irrigation-induced infiltration in the loess deposits at Heifangtai (China), where multi-year wetting-front propagation under continuous irrigation drives the long-term collapse settlement.

4.1.3 Hyperbolic load-settlement response

Figure 5 presents the hyperbolic Kondner–Duncan load-settlement response of the 2 m wide footing in three conditions. The three curves are non-linear and concave-downward, with the asymptote of each curve corresponding to its ultimate bearing capacity q_u and the slope at the origin to its initial subgrade modulus k_i. In the dry state the curve has the steepest initial slope (k_i = 6.0 kPa/mm) and the highest asymptote (q_u = 2,220 kPa); under a service stress of 100 kPa it produces less than 20 mm of settlement and is essentially linear in the working range. Wetting strips 85 percent of this capacity (q_u falls to 332 kPa) and 79 percent of the initial stiffness (k_i falls to 1.25 kPa/mm); the wet curve rises steeply from the origin and asymptotes to its low q_u within the first 50 mm of settlement, indicating a brittle, low-strength medium incapable of supporting moderate commercial loads without large strain. The post-improvement curve sits between the two: k_i is recovered to 2.5 kPa/mm (42 percent of dry) and q_u to 1,612 kPa (73 % of dry condition), and the curve remains nearly linear up to a settlement of about 60 mm before approaching its asymptote.

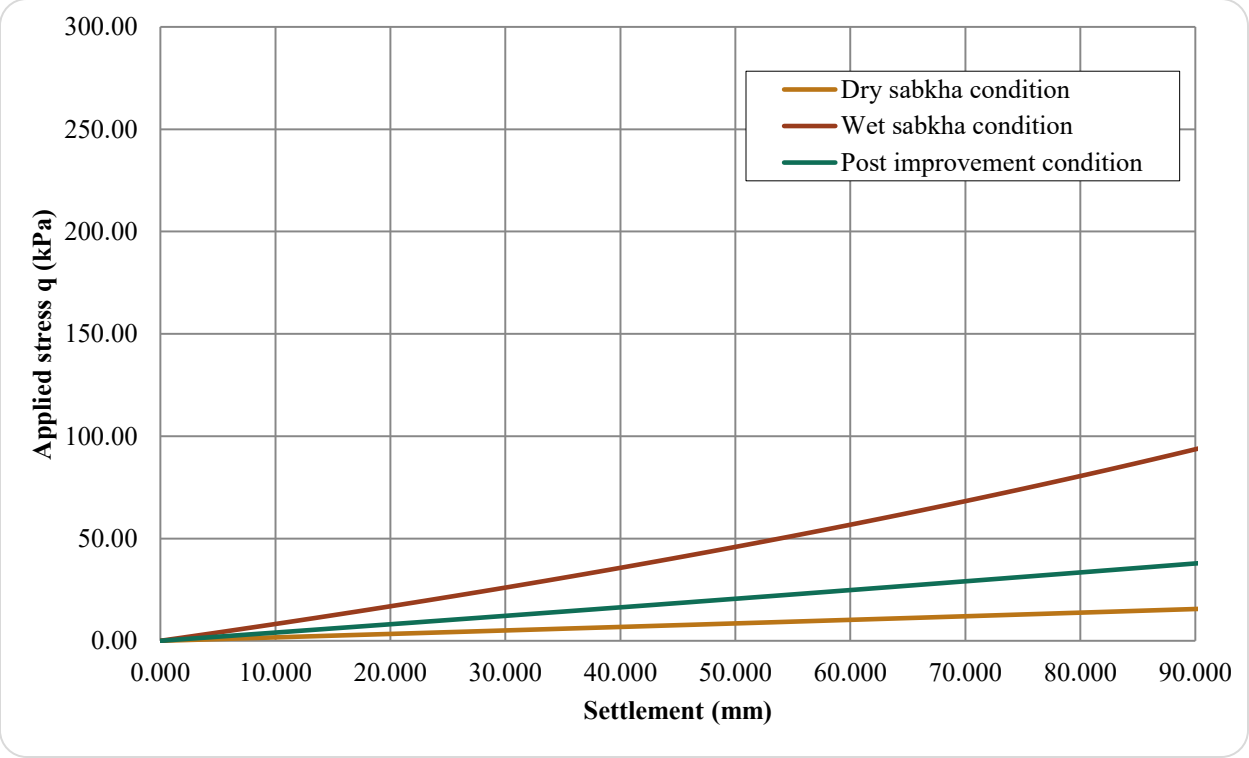


Figure 5. Hyperbolic load-settlement curve

4.1.4 Degradation strength and stiffness behavior

Figure 6 plots the variation of the ultimate bearing capacity q_u and the secant Young's modulus E of the sabkha matrix as a function of volumetric moisture content w over the full hydration range, from the dry state ($w \approx 3$ percent) through to near-saturation ($w \approx 42$ percent). Both q_u and E decrease monotonically and exponentially with increasing w, but the rate of degradation is markedly non-linear: a steep, near-cliff drop occurs between $w = 6$ and 14 percent, where the salt-cemented inter-grain bridges progressively dissolve and the matrix loses its short-range structural strength, followed by a gentler tail beyond $w = 16$ percent where the residual frictional and capillary contributions dominate. The q_u curve falls from 2,220 kPa at $w = 3$ percent to 332 kPa at the wet-state reference of $w \approx 16$ percent (an 85 percent loss) and continues down to 145 kPa at $w = 42$ percent (a 94 percent loss). The E curve shows the same exponential profile, falling from 12,000 kPa to 2,500 kPa over the wet-state interval (a 79 percent loss) and to 1,707 kPa near saturation (an 86 percent loss). The post-improvement state, fixed at the as-built moisture of $w \approx 14$ percent, recovers q_u to 1,612 kPa and E to 5,000 kPa, well above the wet-state lower bound of 332 kPa and 2,500 kPa respectively, because the controlled wetting cycle has already broken the metastable cementation and the consolidation phase has rebuilt frictional contact between the grains. The figure therefore quantifies the engineering trade-off that motivates the innovative scheme: the dry-state design value of 2,220 kPa is essentially unsafe under any uncontrolled wetting, whereas the post-improvement value of 1,612 kPa remains robust against subsequent moisture fluctuations because the matrix is already in its post-collapse equilibrium state.

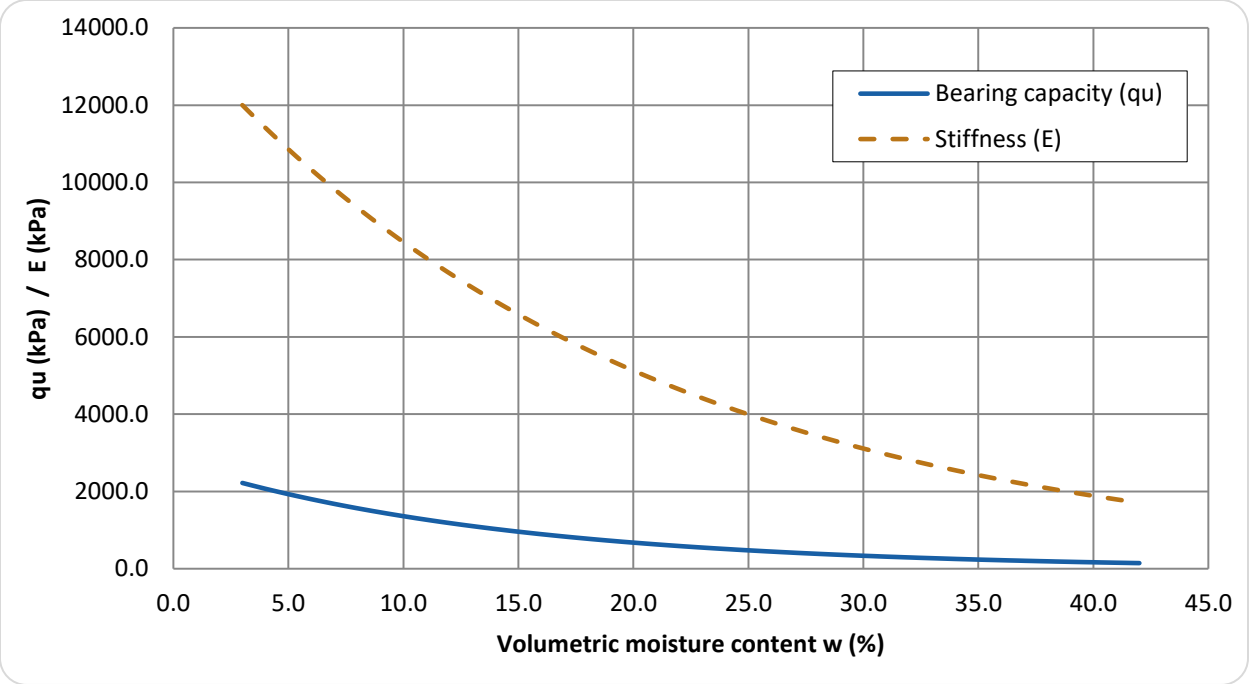


Figure 6. Bearing-capacity and stiffness vs moisture content

The cliff-and-tail shape of the $q_u(w)$ and $E(w)$ envelopes reported here closely matches the laboratory-scale data of Al-Amoudi and Abduljauwad [12] for Arabian Gulf sabkha, of Messad and Moussai [14] for El Hodna sabkha (Algeria), and of Al-Otaibi and Aldaihani [2] for the sabkha and dune-sand deposits of Kuwait, all of which identify a critical moisture window of 6–14 percent volumetric water content over which the cementation dissolves, and the bulk of the strength loss is mobilized. The 85–94 percent loss of bearing capacity reported here lies above the 24–30 percent decrease in bearing capacity that Gaaver [6] measured for soaked Egyptian collapsible soils and is broadly consistent with the high collapse potentials (up to 14.6 percent) reported for undisturbed natural samples, reflecting the relatively weakly cemented reference profile adopted in the present analysis. Garakani et al. [15] demonstrated experimentally that the magnitude of the strength loss correlates strongly with the dissolved-salt content of the wetting fluid, and Niu et al. [17] showed that the soluble-salt content of the matrix controls both the position and the steepness of the cliff portion of the $q_u(w)$ curve, observations that explain why the deeply-saline distilled-water injection used in the innovative scheme produces a deterministic, well-defined collapse pulse rather than the diffuse strength loss seen under uncontrolled rainfall infiltration. The 73 percent post-improvement recovery of the dry-state capacity is also consistent with the irreversible-densification mechanism documented by Pereira and Fredlund [38] for compacted gneiss residual

494 soils, and by Gaaver [6] for Egyptian collapsible soils (where the strength-recovery factor RFSR
495 was measured between 0.53 and 0.75, mean 0.64, between the natural-dry and soaked-compacted
496 states).

497 **4.2 Construction performance of the innovative foundation**

498 Figure 7 visualizes the construction-schedule decomposition of the seven foundation alternatives
499 evaluated in this study, represented as stacked horizontal bars with components: the soil-
500 improvement task, the foundation-construction task, and the superstructure-erection task. The
501 Traditional Pre-Wetting baseline requires 120 days of soil improvement followed by 14 days of
502 foundation construction and 60 days of superstructure erection, all executed serially, for a total
503 critical path T_{cp} = 194 days. The deep-foundation (piling) and chemical-grouting alternatives are
504 slightly lighter on the improvement leg (31 and 28 days, respectively), but their tasks remain serial,
505 yielding critical paths of 105 and 102 days, respectively. Stone Columns (95 days), Lime
506 Treatment (88 days), and Dynamic Compaction (84 days) are executed progressively faster, again
507 in serial order, because the improvement task is the binding constraint on the critical path. The
508 innovative method, by contrast, absorbs the 7-day soil-improvement task entirely into the
509 foundation-construction window: the same crew that places the formwork and reinforcement also
510 installs the nine PVC sleeves and runs the wetting injection, so the improvement leg consumes no
511 calendar time outside the foundation-construction phase. Together with the 14-day foundation-
512 construction window and the standard 60-day superstructure phase, this yields T_{cp} = 74 days, a
513 120-day saving, and a 62 percent compression of the pre-superstructure schedule relative to the
514 Traditional Pre-Wetting baseline, and 10–31 days shorter than the next-fastest alternative.

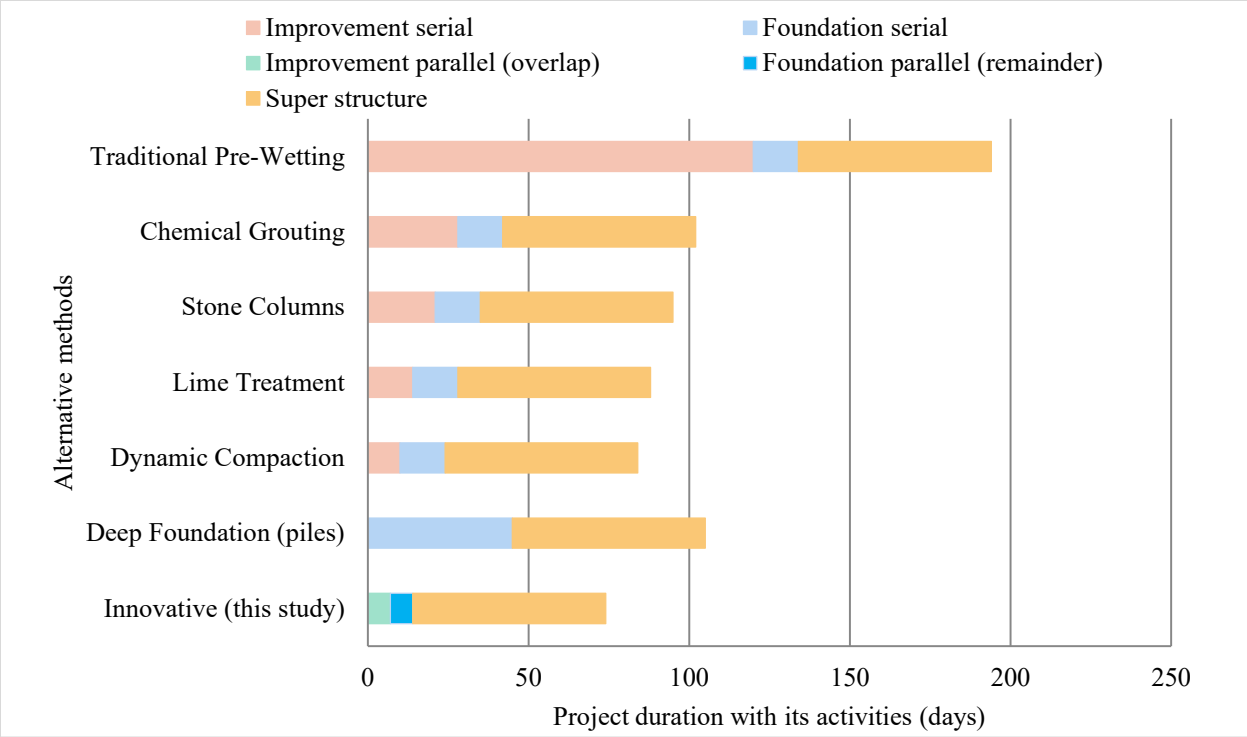


Figure 7. Project-schedule comparison, soil improvement on the critical path vs. overlapped with the foundation

The schedule-overlap principle quantified in Figure 7 is consistent with the lean-construction precepts of Ballard and Howell [8] and with the sustainability-and-constructability framework of Basu, Misra and Puppala [46] for geotechnical engineering, both of which advocate the integration of ground-improvement and foundation tasks into a single concurrent activity wherever the precedence relations permit. Its quantitative application to a collapsible-soil foundation system, however, is novel: the dominant message of Figure 7 is that the soil-improvement task, long held to be the binding constraint on the critical path of arid-region foundations, can be eliminated as a stand-alone activity if the wetting pulse is delivered through the foundation hardware itself. The 62 percent compression reported here is comparable to the project-acceleration gains documented by Raymond et al. [34] in their life-cycle sustainability assessment of geotechnical ground-improvement methods, in which fast-track schemes consistently dominated when assessed against the time-to-revenue criterion, and to the embodied-energy and CO2 emission reductions reported by Shillaber et al. [47] when comparing lower-impact ground-improvement alternatives to material-intensive options on the levee project.

Figure 8 visualizes the seven foundation alternatives on a normalized radar diagram across six performance criteria spanning the engineering, schedule, capital-expenditure, and life-cycle dimensions of the design. Each criterion is rescaled to the unit interval, with 1.0 corresponding to the best-performing alternative for that criterion and 0.0 to the worst, so that the area enclosed by each polygon offers a single visual indicator of overall performance. The assessments were performed with expert panel (nine experts) with experience in construction more than 10 years. The innovative foundation occupies the outermost polygon on the criteria that capture life-cycle value and constructability, net present value, critical-path duration, post-commissioning settlement, and residual collapse probability, while accepting a comparatively low score on the construction-phase settlement criterion, which reflects the deliberate mobilization of approximately 480 mm of wetting-collapse strain under the foundation's own weight before the superstructure is placed. The Traditional Pre-Wetting baseline traces a small, near-central polygon with moderate scores across all axes; Stone Columns and Dynamic Compaction perform reasonably on the engineering axes but are penalized on the schedule and capital-expenditure axes; and Deep Piling and Chemical Grouting deliver competitive engineering performance. The figure makes explicit the multi-criteria trade-off that the innovative scheme resolves: the construction-phase strain (low score on one axis) is the price paid for the dominant scores on every life-cycle and constructability axis, and is, by design, a controlled and pre-commissioning quantity rather than an in-service risk.

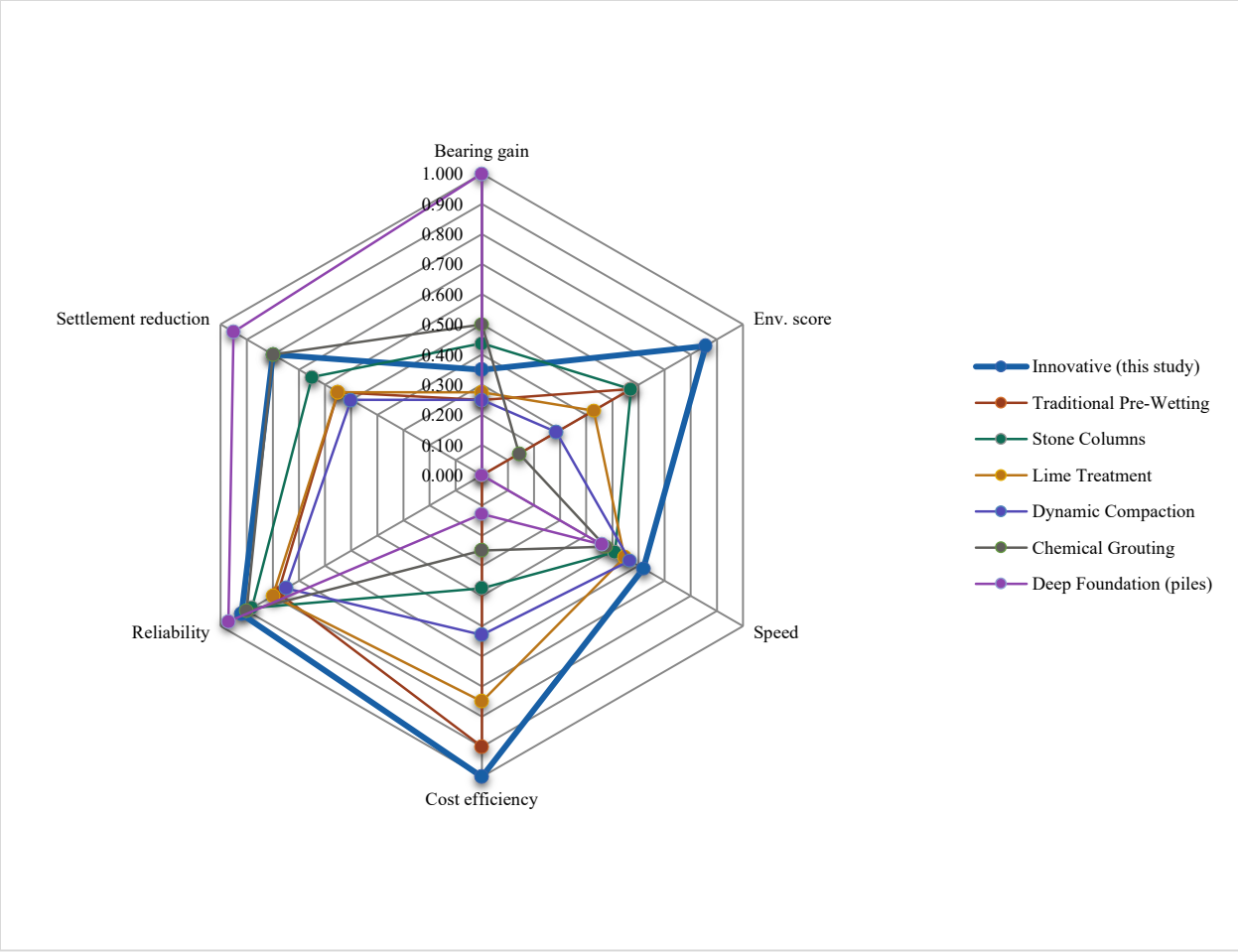


Figure 8. Multi-criteria performance (normalized)

The dominance of the innovative method on the life-cycle and constructability axes of Figure 8 is a direct consequence of integrating the engineering and constructability functions in a single foundation element rather than separating them into a serial improvement-then-foundation sequence. This integrated form mirrors the multi-criteria-dominance results reported by Raymond et al. [34] for sustainability-optimized ground-improvement schemes and by Shillaber et al [47] for energy-and-carbon-optimized foundations, both of which demonstrated that techniques that compress two or more performance criteria simultaneously typically dominate radar-style comparisons. The trade-off that the radar makes explicit, large pre-commissioning collapse strain in exchange for negligible in-service settlement, is the same trade-off identified by Houston et al. [39] and Opukumo et al. [11] as the operational principle of any pre-wetting design for arid-region collapsible soils as the only robust mitigation against in-service inundation events. The innovative foundation breaks this trade-off because the wetting pulse and the foundation construction share

the same calendar window and the same crew, so the engineering benefit is captured without an incremental schedule or capital expenditure cost

5. Conclusion

This paper presents a comprehensive analytical and financial evaluation of a preloaded, premoistened shallow foundation designed specifically for sabkha soils—collapsible, evaporite-cemented deposits widespread across the Arabian Gulf region. The central innovation deliberately triggers wetting-induced collapse under the foundation's own dead weight during a controlled infiltration phase that overlaps temporally with foundation construction, rather than attempting to eliminate collapse risk through conventional ground improvement. Four research questions are addressed.

First, regarding the post-commissioning settlement. The innovative foundation mobilizes approximately 480 mm of collapse settlement, equivalent to the full collapse potential of the 4 m sabkha layer, within 12 days of initiating distilled-water injection through the 3×3 hole array. Total settlement asymptotes at 594 mm and remains essentially flat over the remaining design life. By contrast, a conventional foundation on untreated dry sabkha that experiences accidental in-service inundation suffers an abrupt 480 mm collapse step followed by prolonged wet-state consolidation, terminating at 728 mm, 134 mm larger than the innovative case and, crucially, delivered to the superstructure in service rather than during construction. The analytical predictions were verified by an independent one-dimensional coupled hydro-mechanical numerical model (Richards flow with Barcelona Basic Model loading-collapse formulation), yielding a normalized RMSE of approximately 5.6%, confirming that the uncoupled analytical pipeline is fit-for-purpose.

Second, regarding time-evolving bearing capacity. The hyperbolic load-settlement response shows that dry sabkha exhibits an ultimate bearing capacity of 2,220 kPa and an initial subgrade modulus of 6.0 kPa/mm, which collapse to 332 kPa and 1.25 kPa/mm upon full wetting, resulting in 85% and 79% losses, respectively. The post-improvement state recovers bearing capacity to 1,612 kPa (73% of dry) and stiffness to 2.5 kPa/mm (42% of dry). The degradation curves display a cliff-and-tail shape: a steep loss between 6% and 14% volumetric water content, where salt-cemented bridges dissolve, followed by a gentler tail. The dry-state design value is unsafe under uncontrolled

wetting, whereas the post-improvement value remains robust against subsequent moisture fluctuations.

Third, regarding schedule compression. The schedule overlap principle formalizes that, for the Traditional Pre-Wetting baseline, tasks execute serially over 194 days. For the innovative foundation, the 12-day soil-improvement task is absorbed into the 14-day foundation-construction window, yielding a critical path of only 74 days, a 120-day saving, and 62% compression of the pre-superstructure schedule, with the innovative method 10–31 days faster than the next-fastest conventional alternative. This saving translates directly into avoided site-overhead charges and accelerated revenue generation.

Limitations and future work. Spatial heterogeneity of evaporite cementation was not explicitly modeled. A full three-dimensional hydro-mechanical simulation and physical model tests (1g or centrifuge) are the subject of a companion study.

Principal engineering conclusion. The pre-loaded, pre-moistened foundation converts sabkha's collapse mechanism from a liability into an advantage. By delivering collapse strain under early-construction loading, before the superstructure is placed, the method exhausts the majority of the wetting-induced collapse potential within the treated zone. Some residual risk remains from in-service wetting that penetrates beyond the pre-wetted column (deeper percolation or lateral groundwater rise not intercepted by the hole array); surface- and groundwater management must therefore accompany the foundation design, consistent with the broader collapsible-soil literature reviewed in Section 2. By delivering this collapse strain under self-weight during construction, absorbing improvement into the foundation-construction window, and requiring no cement or chemical additives, the method achieves superior life-cycle financial performance while minimizing residual collapse risk within the treated zone. The schedule overlap principle is general and can be extended to other metastable soil types (loess, gypseous soils, and other salt-cemented deposits) wherever a controlled wetting pulse can be delivered through the foundation hardware itself.

Funding

The authors extend their appreciation to the Nesma and Partners' Chair for Construction Research and Building Technologies for funding this research work.

Data availability

All data generated or analysed during this study are included in this published article [and its supplementary information files].

References

[1] M. Elsawy and A. Lakhouit, "Geotechnical Behaviour of Sandy Sabkha Soils Based on Experimental and Numerical Investigations," *Indian Geotechnical Journal*, vol. 52, pp. 97–112, 2021, doi: 10.1007/s40098-021-00555-2.

[2] F. A. Al-Otaibi and H. M. Aldaihani, "Determination of the collapse potential of sabkha soil and dune sand arid surface soil deposits in Kuwait," *J. Teknol.*, vol. 83, no. 3, pp. 93–100, May 2021, doi: 10.11113/JURNALTEKNOLOGI.V83.14863.

[3] I. Hafhouf and K. Abbeche, "Impact of drying-wetting cycles on shear properties, suction, and collapse of sebkha soils," *Heliyon*, vol. 9, no. 2, Feb. 2023, doi: 10.1016/j.heliyon.2023.e13594.

[4] Bellil, Soumia, and K. Abbeche, "Treatment of a collapsible soil using a bentonite–cement mixture," *Studia Geotechnica et Mechanica*, vol. 40, no. 4, pp. 122–135, 2018, [Online]. Available: https://doi.org/10.1515/xyz-2017-0010

[5] H. Ziani, K. Abbèche, I. Messaoudene, and L. J. Andrade Pais, "Treatment of Collapsible Soils by Additions of Granulated Slag and Natural Pozzolan," *KSCE Journal of Civil Engineering*, vol. 23, no. 3, pp. 1028–1042, Mar. 2019, doi: 10.1007/s12205-019-0051-0.

[6] K. E. Gaaver, "Geotechnical properties of Egyptian collapsible soils," *Alexandria Engineering Journal*, vol. 51, no. 3, pp. 205–210, 2012, doi: 10.1016/j.aej.2012.05.002.

[7] M. G. Jassam, A. H. Abd, and M. A. Hussein, "Effect of Initial Water Content on the Collapsibility of Natural and Cement-Treated Gypseous Soils," *Civil and Environmental Engineering*, vol. 19, no. 2, pp. 610–617, Dec. 2023, doi: 10.2478/cee-2023-0055.

[8] G. Ballard and G. A. Howell, "Lean project management," *Building Research and Information*, vol. 31, no. 2, pp. 119–133, Mar. 2003, doi: 10.1080/09613210301997.

[9] W. Akili and N. Ahmad, "Arabian salt-encrusted flats (sabkha) as building sites," 1987.

[10] O. S. B. Al-Amoudi, "Chemical stabilization of sabkha soils at high moisture contents," *Eng. Geol.*, 1994, doi: 10.1016/0013-7952(94)90009-4.

[11] A. W. Opukumo, C. T. Davie, S. Glendinning, and E. Oborie, "A review of the identification methods and types of collapsible soils," Dec. 01, 2022, *Springer Science and Business Media B.V.* doi: 10.1186/s44147-021-00064-2.

[12] O. Al-Amoudi and S. Abduljauwad, "Compressibility and collapse characteristics of arid saline sabkha soils," *Eng. Geol.*, vol. 39, pp. 185–202, 1995, doi: 10.1016/0013-7952(95)00016-9.

[13] J. Macedo *et al.*, "Geotechnical characterization of collapsible salty sands subjected to monotonic and cyclic loadings – A case study for areas with high seismicity," *Soils and Foundations*, vol. 63, no. 1, Feb. 2023, doi: 10.1016/j.sandf.2022.101252.
[14] A. Messad, B. Moussai, and M. Asce, "Evaluation of the collapsibility of El Hodna sabkha soil-Algeria," *In Geo-China 2016, pp. 278-285. 2016.*.
[15] A. A. Garakani *et al.*, "Effect of road salts on the hydro-mechanical behavior of unsaturated collapsible soils," *Transportation Geotechnics*, vol. 17, pp. 77–90, Dec. 2018, doi: 10.1016/j.trgeo.2018.09.005.
[16] Y. Nie, W. Ni, W. Tuo, H.-M. Wang, K.-Z. Yuan, and Y. Zhao, "Collapsibility deterioration mechanism and evaluation of compacted loess with sodium sulfate under drying–wetting cycles," *Natural Hazards*, vol. 115, pp. 971–991, 2022, doi: 10.1007/s11069-022-05581-8.
[17] L. Niu, W. Ren, A. Zhang, Y. Wang, Z. Liang, and J. Han, "Experimental study on the influence of soluble salt content on unsaturated mechanical characteristics of undisturbed Ili loess," *Bulletin of Engineering Geology and the Environment*, vol. 80, no. 9, pp. 6689–6704, Sep. 2021, doi: 10.1007/s10064-021-02340-0.
[18] S. Ibrahim Shalaby, "Potential Collapse for Sandy Compacted Soil during Inundation," *IJISET-International Journal of Innovative Science, Engineering & Technology*, vol. 4, 2017, [Online]. Available: www.ijiset.com
[19] N. Ali, "Controlling Collapsibility Potential by Partial Soil Replacement," *Global Journal of Research In Engineering*, vol. 16, p., 2016, [Online]. Available: https://consensus.app/papers/controlling-collapsibility-potential-by-partial-soil-ali/4767401a868053978d38c5ad419566e6/
[20] T. Ayadat and A. Hanna, "Design of Foundations Built on a Shallow Depth (Less than 4 m) of Egyptian Macro-Porous Collapsible Soils," *Open Journal of Geology*, vol. 03, no. 03, pp. 209–215, 2013, doi: 10.4236/ojg.2013.33024.
[21] T. Ayadat and A. Hanna, "Encapsulated stone columns as a soil improvement technique for collapsible soil," vol. 9, pp. 137–147, 2005, doi: 10.1680/grim.2005.9.4.137.
[22] A. M. Hasan, S. N. Abdulhamid, and H. H. Ibrahim, "Preliminary experimental investigation on the inundating-induced collapse in collapsible soils improved by encased sand column," *Geomechanics and Geoengineering*, vol. 17, no. 5, pp. 1499–1515, 2022, doi: 10.1080/17486025.2021.1955154.
[23] C. Li *et al.*, "Estimation of the wetting induced settlement of loess soils from the wetting soil-water characteristic curve," *Sci. Rep.*, vol. 14, p., 2024, doi: 10.1038/s41598-024-83258-x.
[24] X. Hou, S. K. Vanapalli, and T. Li, "Wetting-induced collapse behavior associated with infiltration: A case study," *Eng. Geol.*, vol. 258, Aug. 2019, doi: 10.1016/j.enggeo.2019.105146.
[25] W. Yao, C. Li, H. Zhan, and J. Zeng, "Time-dependent slope stability during intense rainfall with stratified soil water content", doi: 10.1007/s10064-018-01437-3/Published.
[26] B. Chen, Q. Ren, F. Wang, R. Zhang, B. Liu, and Y. Jia, "Progressive failure analysis of slope water damage based on improved Green-Ampt infiltration model," Feb. 19, 2021. doi: 10.21203/rs.3.rs-212976/v1.
[27] S. Wang, J. Xu, Q. Wang, and D. Cheng, "Modeling of wetting deformation of coarse saline soil with an improved von Wolffersdorff model," 2020, doi: 10.1007/s10064-020-01855-2/Published.

[28] F. M. Francisca, I. Giomi, and R. J. Rocca, “Inverse analysis of shallow foundation settlements on collapsible loess: Understanding the impact of varied soil mechanical properties during Wetting,” *Comput. Geotech.*, vol. 167, Mar. 2024, doi: 10.1016/j.compgeo.2024.106090.
[29] W. Yao, C. Li, H. Zhan, and J. Zeng, “Time-dependent slope stability during intense rainfall with stratified soil water content,” 2019, doi: 10.1007/s10064-018-01437-3/Published.
[30] M. Fatahizadeh and H. Nowamooz, “Settlement Foundations by Exploring the Collapse of Unsaturated Soils,” *Applied Sciences (Switzerland)*, vol. 14, no. 17, Sep. 2024, doi: 10.3390/app14177688.
[31] Z. xi Yang, X. Kang, S. Wang, D. qing Li, and Y. an Hu, “A simple hypoplastic model for unsaturated soils considering wetting collapse,” *Comput. Geotech.*, vol. 176, Dec. 2024, doi: 10.1016/j.compgeo.2024.106781.
[32] F. d’Onza, “CALIBRATION METHODS OF A CONSTITUTIVE MODEL FOR PARTIALLY SATURATED SOILS: A BENCHMARKING EXERCISE WITHIN THE MUSE NETWORK,” p., 2020, [Online]. Available: https://consensus.app/papers/calibration-methods-of-a-constitutive-model-for-partially-donza-donza/d0a1537d48b255c69cf6d9828b490924/
[33] C. M. Shillaber, J. K. Mitchell, and J. E. Dove, “Energy and Carbon Assessment of Ground Improvement Works. I: Definitions and Background,” *Journal of Geotechnical and Geoenvironmental Engineering*, vol. 142, no. 3, Mar. 2016, doi: 10.1061/(asce)gt.1943-5606.0001410.
[34] A. J. Raymond, J. T. DeJong, A. Kendall, J. T. Blackburn, and R. Deschamps, “Life Cycle Sustainability Assessment of Geotechnical Ground Improvement Methods,” *Journal of Geotechnical and Geoenvironmental Engineering*, vol. 147, no. 12, Dec. 2021, doi: 10.1061/(asce)gt.1943-5606.0002646.
[35] O. S. B. Al-Amoudi, “Chemical stabilization of sabkha soils at high moisture contents,” *Eng. Geol.*, vol. 36, no. 3–4, pp. 279–291, 1994.
[36] M. A. Al-Shamrani and A. W. Dhowian, “Characterization of secondary compression behavior of Sabkhasoils,” *Eng. Geol.*, vol. 48, no. 1–2, pp. 19–41, 1996.
[37] D. G. Fredlund and A. Xing, “Equations for the soil-water characteristic curve,” *Canadian geotechnical journal*, vol. 31, no. 4, pp. 521–532, 1994.
[38] B. H. Jose F Pereira and D. G. Fredlund, “VOLUME CHANGE BEHAVIOR OF COLLAPSIBLE COMPACTED GNEISS SOIL,” 2000.
[39] S. L. Houston, W. N. Houston, C. E. Zapata, and C. Lawrence, “Geotechnical engineering practice for collapsible soils,” 2000.
[40] Celia, Michael A., Efthimios T. Bouloutas, and Rebecca L. Zarba., “A general mass-conservative numerical solution for the unsaturated flow equation,” *Water resources research* , vol. 26, no. 7, pp. 1483–1496, 1990.
[41] E. E. Alonso, A. Gens, and A. Josa, “A constitutive model for partially saturated soils,” *Géotechnique*, vol. 40, no. 3, pp. 405–430, 1990.
[42] J. M. Duncan and C.-Y. Chang, “Nonlinear analysis of stress and strain in soils,” *Journal of the soil mechanics and foundations division*, vol. 96, no. 5, pp. 1629–1653, 1970.
[43] J. Boussinesq, *Application des potentiels à l’étude de l’équilibre et du mouvement des solides élastiques*. Gauthier-Villars, Imprimeur-Libraire, 1885.
[44] M. Budhu, *Soil Mechanics Fundamentals*. John Wiley & Sons, 2015.

[45] H. H. Adem and S. K. Vanapalli, “Review of methods for predicting in situ volume change movement of expansive soil over time,” Feb. 01, 2015, *Chinese Academy of Sciences*. doi: 10.1016/j.jrmge.2014.11.002.
[46] D. Basu, A. Misra, and A. J. Puppala, “Sustainability and geotechnical engineering: perspectives and review,” *Canadian geotechnical journal*, vol. 52, no. 1, pp. 96–113, 2015.
[47] C. M. Shillaber, J. K. Mitchell, and J. E. Dove, “Energy and Carbon Assessment of Ground Improvement Works. II: Working Model and Example,” *Journal of Geotechnical and Geoenvironmental Engineering*, vol. 142, no. 3, Mar. 2016, doi: 10.1061/(asce)gt.1943-5606.0001411.

Supplementary Files

This is a list of supplementary files associated with this preprint. Click to download.

- Bearingcapacityandstiffnessvsmoisturecontent.xlsx
- Multicriteriaperformancenormalized.xlsx
- Timehistorysettlementoftheinnovativefoundationandfoundationindryandwetconditions.xlsx
- Projectschedulecomparisonsoilimprovementonthecriticalpathvs.overlappedwiththefoundation.xlsx
- Hyperbolicloadsettlementcurve.xlsx